CEAI, Vol.22, No.2 pp. 23-32, 2020 Printed in Romania

Advanced Gain-Scheduled Control of A DFIG based on a H-Darrieus Wind Turbine for Maximum Power Tracking and Frequency Support

Josephat Machoka Bundi*, Xiaojun Ban*, David Wafula Wekesa, Yue Sun***

**Center for Control theory and Guidance Technology, Harbin Institute of Technology, 150001, Harbin, PR China (e-mail: logan.machoka@ hit.edu.cn, banxiaojun @ hit.edu.cn,15B304004@hit.edu.cn)*
***Department of Physics, Multimedia University of Kenya, 15653-00503, Nairobi, Kenya (e-mail: dwekesa@mksu.ac.ke)*

Abstract: Voltage dips are a major problem in grid connected turbines as they cause voltage imbalance in the grid and are likely to cause a shutdown in the turbine operation momentarily. Wind turbines such as Vertical axis wind turbines (VAWTs) have poor self-starting characteristics. In addition, a large breaking mechanism will require a long time to settle back to steady state operation. A doubly fed induction generator (DFIG) based VAWT plant offers great flexibility against highly fluctuating turbulent winds of urban set-ups. This paper proposes a control mechanism that ensures frequency support to the grid and also protects the VAWT from severe conditions of the grid voltage imbalance. In this work, A LPV, gain scheduled control approach based on linear matrix inequalities (LMIs) is applied for the vector control of small scale VAWT based doubly fed induction generator (DFIG). The results show satisfactory performance and response of the proposed control system. The study algorithms were coded and implemented in MATLAB R2018a & Simulink. Hopefully, the study findings will provide more insight into the application of doubly fed induction generators with small-scale vertical axis wind turbines.

Keywords: Doubly fed induction generator, gain scheduled control, Linear parameter varying, Vertical axis wind turbine, Vector control

1. INTRODUCTION

Vertical axis wind turbines (VAWTs) infamous for their efficiency in areas with turbulent and fluctuating wind flows (Nguyen and Metzger, 2017; Wekesa et al., 2016). This is a common phenomenon in areas with many obstacles to wind flow such as urban and sub-urban environments. Their insensitiveness to the direction of wind also makes them a suitable candidate for application in such conditions. Furthermore, VAWTs have a further stability advantage because the structure allows for the generator to be placed at the base.

Doubly fed induction generators (DFIGs) on the other hand are popular for wind power generation because of their capability for variable speed operation, small power converters, independent active and reactive power control and minimized power losses (Houpis and Garcia-Sanz, 2012; Merabet et al., 2018; Polinder et al., 2013). Notwithstanding, the DFIG holds its own challenges which emerge in the overall control for smooth and efficient operation. Conventionally, control of grid connected DFIGs is effected via stator-voltage oriented or stator flux oriented vector control. This schemes allow for decoupled control of active and reactive power through the decoupled currents in the d-q reference frame. Tracking performance is highly dependent of the exact machine parameters and uncertainties in the system (Merabet et al., 2018). Hence this demands a good and robust control algorithm to allow for agreeable performance.

Another advantage to the DFIGs lies in their ability to generate power both below and above synchronous speeds. This makes them a promising solution for application along with small vertical axis wind turbines which are known to operate in fluctuating and turbulent wind conditions that are characteristics of urban environments. Despite the overall advantages to such a configuration, the challenge exists in getting the most suitable control approach to guarantee good performance along the entire operation trajectory and also to allow for a smooth operation and integration to the micro-grid.

In response to grid challenges such as voltage dips and frequency drops (Ramtharan et al., 2007), the turbines are required to be adamant to these changes in terms of their operation efficiency and also be able to give support to the grid by quick adaptations. This is a complex task since the turbine faces multiple uncertainties and requirements for pitch control, maximum power tracking and power supply-demand balance.

Various control schemes have been developed for improvement of DFIG-based wind turbine systems however, configurations involving VAWTs have only started to receive increased interest in the recent past. Cardenas et. al. (Cárdenas et al., 2013) gave a review on various control systems that were applied for DFIGs employed in wind turbines for connection to balanced and unbalanced grids, stand-alone operation, sensorless control, frequency support by DFIGs and low-voltage ride through (LVRT). Tien et. al. (Tien et al., 2016) proposed a LPV control for DFIG and exploited the feature of discretization for dynamic and robust performance for the mechanical speed variations. The work however only focused on the DFIG and there was no connection to any specific turbine. An LPV approach proposed by (Wang and Weiss, 2014) was aimed at frequency support and maximization of power, on the out loop of the vector control structure, and fast current tracking on the inner loop current loop. Other literature addressing the control of DFIGs include (Merabet et al., 2018; Wang et al., 2016) where they applied

H-infinity control for robust current control to suppress uncertainties due to grid voltage distortions and a sliding mode control law for dc-link voltage regulation under different operating conditions. This studies however, focus on the grid side control as opposed to the rotor side control. Figure 1 shows a VAWT based wind farm control scheme.

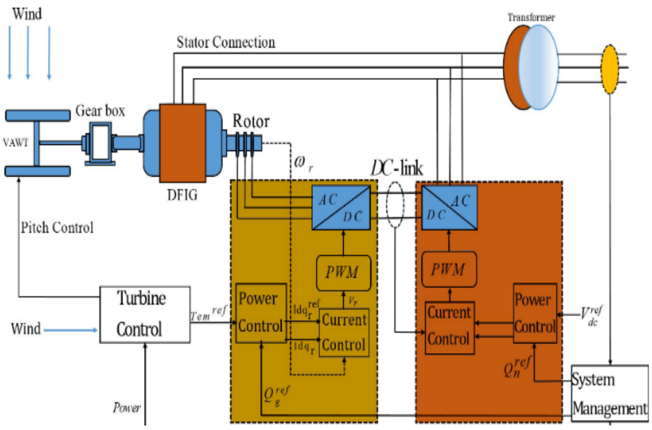

Fig. 1.VAWT based wind energy conversion system.

blades as in (Inthamoussou et al., 2014; Inthamoussou et al., 2016). These studies gave a general approach based on horizontal axis wind turbines (HAWTs) whose dynamics are different to VAWTs. Most studies concerning VAWTs are structural oriented (Cheng et al., 2017; Danao et al., 2014; Onol and Yesilyurt, 2017; Rezaeiha et al., 2017; Wekesa et al., 2016; Wong et al., 2017) as opposed to control oriented where so little has been done. Some of the works addressing control of VAWTs, particularly small-scale include (Abdalrahman et al., 2017; Breslan et al., 2016). For instance, Abdalrahman et. al. (Abdalrahman et al., 2017), used a multilayer perception layer (MPL) artificial neutral network for control of the pitch angle of a small-scale stand-alone VAWT.

The major contribution of this paper is to study the control of small scale vertical axis wind plants based on doubly fed induction generators. This subject has received minimal attention in the recent past yet it is significant in furthering the efforts of renewable energy availability close to where it is produced. The paper thus proposes the torque control of a small scale vertical axis wind turbine (VAWT) based on doubly fed induction generators using advanced linear matrix inequalities technique. The control structure follows a quasi-maximum power point (MPPT) paradigm used to generate maximum energy from the turbine. The work considers variable wind speeds that take into account the gusts and turbulent wind conditions realized in Marsabit, a rural-urban town in eastern Kenya. By including the drive train dynamics, this accounts for realistic conditions for any admissible perturbations in the working and performance of a VAWT. Furthermore, modifications are added to the MPPT strategy to automatically scale down excessive power to a demanded power level which is normally manually operated according to (Inthamoussou et al., 2016). Additionally, the robustness of the self-scheduled controller is tested for frequency support in case of possible voltage-dips. The controller is validated against conventional PID control which is normally used as a base controller. Figure 2 gives a representation of the dynamic rotor side control for a DFIG. The rest of the paper is organized into (II) Modelling of the system (III) LPV description of the DFIG (IV) Gain scheduling numerical method (V) Proposed modifications and (VI) Results and Discussion.

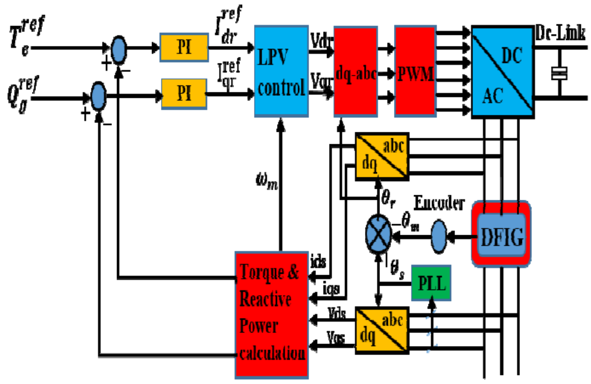

Fig. 2. Rotor side control structure (Tien et al., 2016).

2. SYSTEM MODELLING

2.1 VAWT–Aerodynamic Model

The turbine is a flexible structure comprising of distinct parts coupled to form a single system. These include the rotors, the shafts, gearbox, generator and converter. The turbine blades (rotors) interact with wind developing a torque called aerodynamic torque T_r . The aerodynamic torque is derived according to (Abdalrahman et al., 2017; Inthamoussou et al., 2016):

$$T_r = \frac{P_r}{\Omega_r} = \frac{0.5\rho A v^3 C_p(\lambda,\beta)R}{v\lambda} \tag{1}$$

which can also be written as (Wekesa et al., 2017; Wekesa et al., 2016) .

$$T_r = 0.5\rho A v^2 C_T(\lambda,\beta)R \tag{2}$$

The vertical axis wind turbine parameters are as provided in table (1) below following a VAWT experiment conducted by (Balduzzi et al., 2016) and CFD simulations carried out by (Abdalrahman et al., 2017).

Table 1. Features of the VAWT.

Feature for VAWT	Value	Feature for VAWT	Value
Rotor radius R	0.85 m	Tip speed ratio, λ	1,1.7,2,2.5, 3.3
Number of blades	3	Turbine inertia, J_r	136.5525 kgm^2
Blade profile	NACA 0018	Shaft stiffness, K_s	22.05 Nm / rad
Chord, c (m)	0.24	Generator inertia, J_g	0.2000 kgm^2
Aspect Ratio (AR)	12	Shaft damping coefficient, B_s	0.0150 Nms/rad

2.2 Two Mass Drive Train Model

The drive train comprises of the high and low speed transmission shafts and gearbox between the rotor and the generator. In this work, a two-mass mechanical system is adopted. The difference between the rotor angular deviation θ_r and the low speed shaft angular deviation θ_{ls} yields θ_s, the angular difference (Boukhezzar and Siguerdidjane, 2010):

$$\theta_r - \theta_{ls} = \theta_s \tag{3}$$

The differential angular difference is obtained as follows (Boukhezzar and Siguerdidjane, 2010) :

$$\dot{\theta} = \Omega_r - \Omega_{ls} = \Omega_r - \frac{\Omega_g}{N_g} \tag{4}$$

where the terms Ω_r, Ω_{ls}, Ω_g, N_g represent rotor speed, low speed shaft speed, generator speed and gearbox ratio, respectively.

The aerodynamic torque works against the inertia of the turbine, the friction factors in the moving parts and the shaft torque referred from the generator. This is expressed numerically (Boukhezzar and Siguerdidjane, 2010) as:

$$J_r \dot{\Omega}_r = T_r - T_{ls} - B_r \Omega_r \tag{5}$$

where the low speed shaft torque T_{ls} is expressed as (Boukhezzar and Siguerdidjane, 2010)

$$T_{ls} = K_{ls}(\theta_r - \theta_{ls}) + B_{ls}(\Omega_r - \Omega_{ls}) \tag{6}$$

Substituting (3) into (6) and (6) into (5) then factoring out leads to (7) with $\Omega_{ls} = \Omega_g / N_g$

$$J_r \dot{\Omega}_r = T_r - K_{ls}\theta_{ls} - (B_{ls} + B_r)\Omega_r + B_{ls}\frac{\Omega_g}{N_g} \tag{7}$$

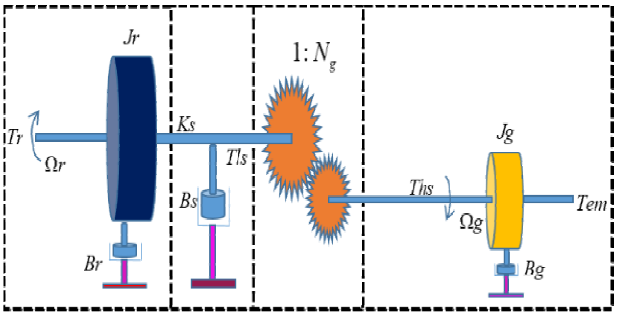

Fig. 3. Two mass drive train scheme.

Figure 3 shows a two degree of freedom scheme of a drive train used for the set-up.

The coupling between the generator and the high speed shaft is as in (8) (Boukhezzar and Siguerdidjane, 2010):

$$J_g \dot{\Omega}_g = T_{hs} - B_g \Omega_g - Tem \tag{8}$$

where the terms T_{hs}, B_g and Tem are the high speed shaft torque, generator damping coefficient, and electromagnetic torque respectively. Equation (8) is modified by substituting T_{hs} with $T_{hs} = T_{ls}/N_g$ to obtain (9) (Boukhezzar and Siguerdidjane, 2010) :

$$J_g \dot{\Omega}_g = \frac{K_{ls}}{N_g}\theta_s + \frac{B_{ls}}{N_g}\Omega_r - \left(\frac{B_{ls}}{N_g^2} + B_g\right)\Omega_g - Tem \tag{9}$$

2.3 Modeling of the DFIG in the d-q Frame

The dynamics of the DFIG expressed in a synchronously rotating d-q frame for the rotor and stator sides are given in (Vas, 1998) as;

$$\begin{cases} v_{sd} = R_s i_{sd} - \Omega_s \psi_{sq} + \dfrac{d\psi_{sd}}{dt} \\ v_{sq} = R_s i_{sq} + \Omega_s \psi_{sq} + \dfrac{d\psi_{sq}}{dt} \end{cases} \tag{10}$$

$$\begin{cases} v_{rd} = R_r i_{rd} - (\Omega_s - \Omega_r)\psi_{rq} + \dfrac{d\psi_{rd}}{dt} \\ v_{rq} = R_r i_{rq} + (\Omega_s - \Omega_r)\psi_{rd} + \dfrac{d\psi_{rq}}{dt} \end{cases} \tag{11}$$

where v_{sd} and v_{sq} are the $d-q$ stator voltages, R_s is the stator resistance, i_{sd} and i_{sq} are the $d-q$ stator currents , ψ_{sq} and ψ_{sd} are the $d-q$ stator fluxes, v_{rd} and v_{rq} are the $d-q$ rotor voltages, R_r is the rotor voltage, i_{rd} and i_{rq} are the $d-q$ rotor currents, ψ_{rd} and ψ_{rq} are the d-q rotor fluxes, Ω_s is the synchronous angular speed, Ω_r is the rotor speed and the slip angular speed is represented as $(\Omega_s - \Omega_r)$.

The stator and rotor fluxes are expressed in terms of the rotor and stator currents below (Vas, 1998)

$$\begin{cases} \psi_{sd} = L_s i_{sd} + L_m i_{rd} \\ \psi_{sq} = L_s i_{sq} + L_m i_{rq} \\ \psi_{rd} = L_r i_{rd} + L_m i_{sd} \\ \psi_{rq} = L_r i_{rq} + L_m i_{sq} \end{cases} \tag{12}$$

where $L_s = L_{\sigma s} + L_m$, $L_r = L_{\sigma r} + L_m$ are the total inductance of stator and rotor coils (Smajo and Vukadinovic, 2008) whereas $L_{\sigma s}, L_{\sigma r}, L_m$ are the stator leakage, rotor leakage and mutual inductances respectively.

Adopting the stator voltage orientation where the stator voltage is aligned with the d-axis of the rotating reference frame (Li et al., 2009), the stator active and reactive powers, P_s and Q_s respectively can be given by

$$\begin{cases} P_s = -\dfrac{3}{2}\dfrac{L_m}{L_s} V_s i_{rd} \\ Q_s = \dfrac{3}{2}\left(\dfrac{V_s \psi_s}{L_s} - \dfrac{L_m}{L_s} V_s i_{rq}\right) \end{cases} \tag{13}$$

where V_s is the stator voltage and ψ_s is the stator flux.

Equation (13) can be rewritten as (14) (Merabet et al., 2018)

$$\begin{bmatrix} P_s \\ Q_s \end{bmatrix} = \begin{bmatrix} 0 & -\frac{3}{2}\frac{L_m}{L_s}V_s \\ -\frac{3}{2}\frac{L_m}{L_s}V_s & 0 \end{bmatrix} \begin{bmatrix} i_{rq} \\ i_{rd} \end{bmatrix} + \begin{bmatrix} 0 \\ \frac{3}{2}\frac{V_s\psi_s}{L_s} \end{bmatrix} \tag{14}$$

It can be deduced from (14) that active and reactive powers can be decoupled and controlled separately by means of the *d–q* rotor currents. The DFIG, electromagnetic torque, is obtained from (13) as

$$T_{em} = p\frac{P_s}{\Omega_g} = -\frac{3}{2}p\frac{L_m}{L_s}(\psi_{sq}I_{dr}) \tag{15}$$

where p is the number of pole pairs and Ω_g is the generator rotor mechanical speed. Refer to (Merabet et al., 2018) for more details on the derivation of the DFIG in the d-q frame for interested readers.

2.4 LPV Model of the DFIG

The dynamics of the DFIGs can be estimated by the following 4th order LPV description according to Wang et al. 2017 (Wang et al., 2016) based on the stator voltage orientation. The varying parameter is selected to be the mechanical angular velocity of the rotor Ω_g which leads to an affine system with two vertices according to equation (17) . The rotor speed is time varying and can be measured online. It varies within up to 1/3 of the synchronous speed ω_S. Hence it can be represented as $\Omega_g=\omega_S(1+P_\Omega\delta_\Omega(t))$ with $P_\Omega=0.3$ and $-1\le\delta_\Omega\le 1$. This leads to the affine system

$$\begin{aligned} \dot{x} &= (A_0x+\delta_\Omega A_1x)+Bv+Bu \\ y &= Cx \end{aligned} \tag{16}$$

$$\begin{aligned} A_1 &= A_0+\delta_{min}A_1 \\ A_2 &= A_0+\delta_{max}A_1 \end{aligned} \tag{17}$$

The constant time-invariant matrices A_0 , A_1 are

$$A_0 = \begin{bmatrix} -(\frac{a+1}{T_r}+\frac{a}{T_s}) & 0 & \frac{a}{L_mT_s} & -\frac{a\omega_s}{L_m} \\ 0 & -(\frac{a+1}{T_r}+\frac{a}{T_s}) & \frac{a\omega_s}{L_m} & \frac{a}{L_mT_s} \\ \frac{L_m}{T_s} & 0 & -\frac{1}{T_s} & \omega_s \\ 0 & \frac{L_m}{T_s} & -\omega_s & -\frac{1}{T_s} \end{bmatrix}$$

$$A_1 = \begin{bmatrix} 0 & -\omega_s p_s & 0 & -\frac{a\omega_s p_\Omega}{L_m} \\ \omega_s p_s & 0 & \frac{a\omega_s p_\Omega}{L_m} & 0 \\ 0 & 0 & 0 & 0 \\ 0 & 0 & 0 & 0 \end{bmatrix} \tag{18}$$

where $a = \frac{Lm^2}{LsLr-Lm^2}$

The rest of the state matrices that are not affected by the affine dependence on the parameters are given by (19) and (20)

$$B_1 = \begin{bmatrix} -\frac{1-\sigma}{\sigma L_m} & 0 & 0 & 0 \\ 0 & -\frac{1-\sigma}{\sigma L_m} & 0 & 0 \\ 1 & 0 & 0 & 0 \\ 0 & 1 & 0 & 0 \end{bmatrix} \quad B_2 = \begin{bmatrix} \frac{1}{\sigma L_r} & 0 \\ 0 & \frac{1}{\sigma L_r} \\ 0 & 0 \\ 0 & 0 \end{bmatrix}$$

(19)

$$C_1 = \begin{bmatrix} -1 & 0 & 0 & 0 \\ 0 & -1 & 0 & 0 \end{bmatrix} \qquad D_1 = \begin{bmatrix} 0 & 0 & 1 & 0 \\ 0 & 0 & 0 & 1 \end{bmatrix} \tag{20}$$

The states x, the outputs z, y, the exogenous input w and the controller outputs u are given as follows

$$x = \begin{bmatrix} I_{dr} \\ I_{qr} \\ \phi_{sd} \\ \phi_{sq} \end{bmatrix}, \quad z = \begin{bmatrix} I_{dr} \\ I_{qr} \\ e_{dr} \\ e_{qr} \end{bmatrix}, \quad w = \begin{bmatrix} V_{ds} \\ V_{qs} \\ I_{dr}^{ref} \\ I_{qr}^{ref} \end{bmatrix}, \quad y = \begin{bmatrix} I_{dr} \\ I_{qr} \end{bmatrix}, \quad u = \begin{bmatrix} V_{dr} \\ V_{qr} \end{bmatrix} \tag{21}$$

The plant augmentation with the weighting functions are obtained following the steps in (Østergaard et al., 2009) and is represented as in fig 4.

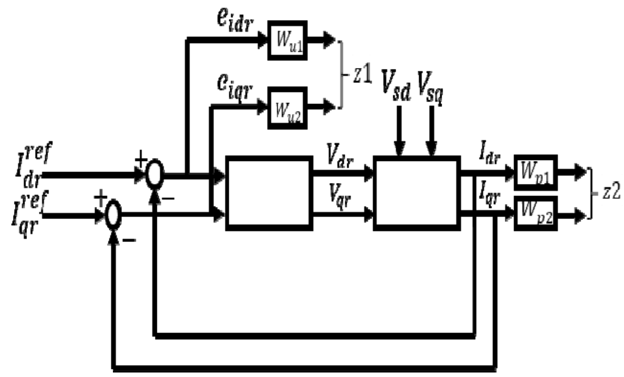

Fig. 4. Weighted system interconnection.

3. NUMERICAL METHOD

3.1 Convex LMI Optimization

Using the theory in (Apkarian and Adams, 2000; Apkarian et al., 1995, Gu et al., 2005, Willems, 1971) and with

$$\begin{bmatrix} X & I \\ I & Y \end{bmatrix} > 0 \tag{22}$$

two steps are followed in the controller development.

1) offline computation of the vertex controller matrices $K_j=(A_{kj}, B_{kj}, C_{kj}, D_{kj})$ which are obtained from solving the factorization problems of (23) and (24).

$$\begin{bmatrix} XA_j+\hat{B}_{Kj}C_{2j}+(XA_j+\hat{B}_{Kj}C_{2j})^T & (\hat{A}^T_{Kj}+A_j)^T & XB_{1j}+\hat{B}_{Kj}D_{21j} & (C_{1j})^T \\ \hat{A}^T_{Kj}+A_j & A_jY+B_{2j}\hat{C}_{Kj}+(A_jY+B_{2j}\hat{C}_{Kj})^T & B_{1j} & (C_{1j}Y+D_{12j}\hat{C}_{Kj})^T \\ (XB_{1j}+\hat{B}_{Kj}D_{21j})^T & B^T_{1j} & -\gamma I & D^T_{11j} \\ C_{1j} & C_{1j}Y+D_{12j}\hat{C}_{Kj} & D_{11j} & -\gamma I \end{bmatrix} \quad (23)$$

$$I - XY = NM^T \quad (24)$$

and then solving for

$$A_{kj} = N^{-1}(\hat{A}_{kj} - XA_jY - \hat{B}_{kj}C_{2j}Y - XB_{2j}\hat{C}_{Kj})M^{-T} \quad (25)$$

$$B_{kj} = N^{-1}\hat{B}_{kj} \quad (26)$$

$$C_k = (\hat{C}_k - D_kC_2Y)M^{-T} \quad (27)$$

2) online computation that requires the measurement of the parameter $\theta(t)$ and computation of its convex de-composition as in (28)

$$\theta(t) = \alpha_1\theta_1 + \alpha_2\theta_2 + \ldots + \alpha_r\theta_r \quad (28)$$

where $\sum_{j=1}^{r} \alpha_j = 1$ and $\alpha_j > 0$.

Finally, with the results obtained by the above steps, the matrices of the controllers are computed as a convex combination of the vertex controllers given as:

$$K(\theta) = \begin{bmatrix} A_K & B_K \\ C_K & 0 \end{bmatrix}(\theta) = \sum_{j=1}^{r} \alpha_j \begin{bmatrix} A_{kj} & B_{kj} \\ C_{kj} & 0 \end{bmatrix} \quad (29)$$

3.2 System Modifications

The system is modified to track the maximum power locus but also to limit power to equal the demanded power in the event that most loads across the consumption line have been shut down. This is mostly done manually by plant operators in commercial schemes (Inthamoussou et al., 2016).

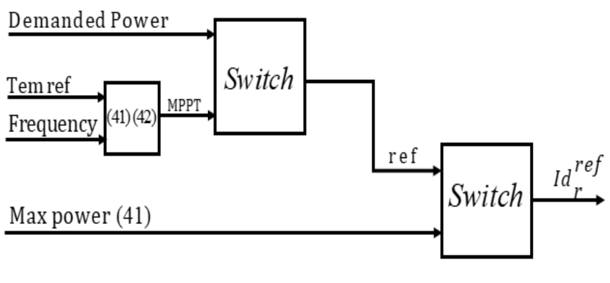

Fig. 5. Electrical torque reference calculation.

This part illustrates a proposed scheme for low voltage ride through (LVRT) in the grid by offering primary frequency support and, for protection of the speed of the VAWT which would otherwise have difficulties in returning to steady state operation under big frequency fluctuations. Figure 5 illustrates the control signal determination for automatic operation of a power plant. This application will be of help to both stand-alone and grid-connected turbines.

LVRT grid frequency support is embedded into the maximum power point tracking (MPPT) quadratic law (30). A PID regulator is used to track and compare the measured grid frequency with the reference grid frequency. When the difference between the measured and reference frequency signals is zero, the signal follows the conventional MPPT locus. A drop in the line frequency triggers a compensation that in turn leads to an increase in the electromagnetic torque. This forces the VAWT to transfer some of the kinetic energy stored in form of inertia to the generator and to the grid to compensate for the voltage dip.

$$T_g = 0.5\rho AC_{p\_mx}\Omega_r^2 R^3/\lambda_{opt}^3 \quad (30)$$

A switch is connected between the power demanded and the MPPT law. Whenever the power demanded is less than the MPPT provides, the switch is set to select the demanded power profile. Another switch is set to offer speed protection in the case that the rotor speed goes below a specified value.

Speed protection can be according to (31) and (32) below

$$Tem_{mx} = -\frac{3}{2}p\frac{Lm}{Ls}F_sIdr_{mx} = -\frac{3}{2}p\frac{Lm}{Ls}\frac{\hat{V}_g}{\omega_s}Idr_{mx} \quad (31)$$

$$Idr_{max} = \frac{Tem_{mx}}{-1.5p\frac{Lm\hat{V}_g}{Ls\omega_s}} \quad (32)$$

Thus whenever the demanded current Idr is greater than Idr_{mx} due to an extended voltage dip, the mechanism momentarily disconnects the conventional reference torque requirement and connects a zero torque reference to allow for speed recovery. For frequency support, V_g in (31) is expressed as (33)

$$V_g ; 2\pi f_g F_s / p \quad (33)$$

where f_g is the grid frequency and p is the number of pole pairs.

4. RESULTS AND DISCUSSION

The subsequently obtained results are obtained by simulations using MATLAB & SIMULINK R2018a. The computer used is of 16GB RAM and a dual core processor. The vertical axis wind turbine (VAWT) is modelled as described above and connected to the DFIG using a two mass drive-train. The control employs the stator voltage oriented control (SVOC) which is more accurate compared to stator flux oriented control (SFOC) according to (Li et al., 2009). The rotor side control of the wound rotor induction machine is effected according to Fig 2.

The controller designed is evaluated using an integrated transient simulation system developed using the Sim Power systems toolbox of Simulink. The grid representation is with a three phase 50 Hz, 380 V line-line programmable voltage source applied to the stator directly. The three-phase rotor voltage is controlled via the V_{rd} and V_{rq} voltages through the pulse width modulation and the rotor side converter which comprises of ideal switches. The controlled three-phase rotor voltage is obtained by *dq-to-abc* park transformation according to the stator voltage space vector position and rotor position obtained by a simplified PLL. The moment of inertia of the DFIG is $0.2\,kgm^2$, the stator and rotor resistances are $0.72\,\Omega$ and $0.75\,\Omega$ respectively, mutual inductance, 0.0858 H and the stator and rotor leakage inductances are 0.0916 H and 0.918 H respectively. The weighting functions used are Wp=[Wp1 0; 0 Wp2] and $Wu=\begin{bmatrix} Wu1 & 0; & 0 & Wu2\end{bmatrix}$ as in (34)

$$Wp=\begin{bmatrix} \frac{2800}{2s+100} & 0 \\ 0 & \frac{2800}{2s+100} \end{bmatrix},\quad Wu=\begin{bmatrix} \frac{0.0001s}{s+100} & 0 \\ 0 & \frac{0.0001s}{s+100} \end{bmatrix} \tag{34}$$

The PI gains are suitably chosen as kp_id=59.2500, kp_iq=59.2500, ki_id=7.8721e+04, ki_iq=7.8721e+04

4.1 Tracking Response of the Self-Scheduled Controller

Figure 6 shows the tracking response of the self-scheduled controller. In this set-up, the VAWT is disconnected and a constant torque is applied to the DFIG. This is because the dynamics of the VAWT are slower than the DFIG dynamics.

To test for robustness of the controller to quick variations of the plant parameters, such a set-up is necessary.

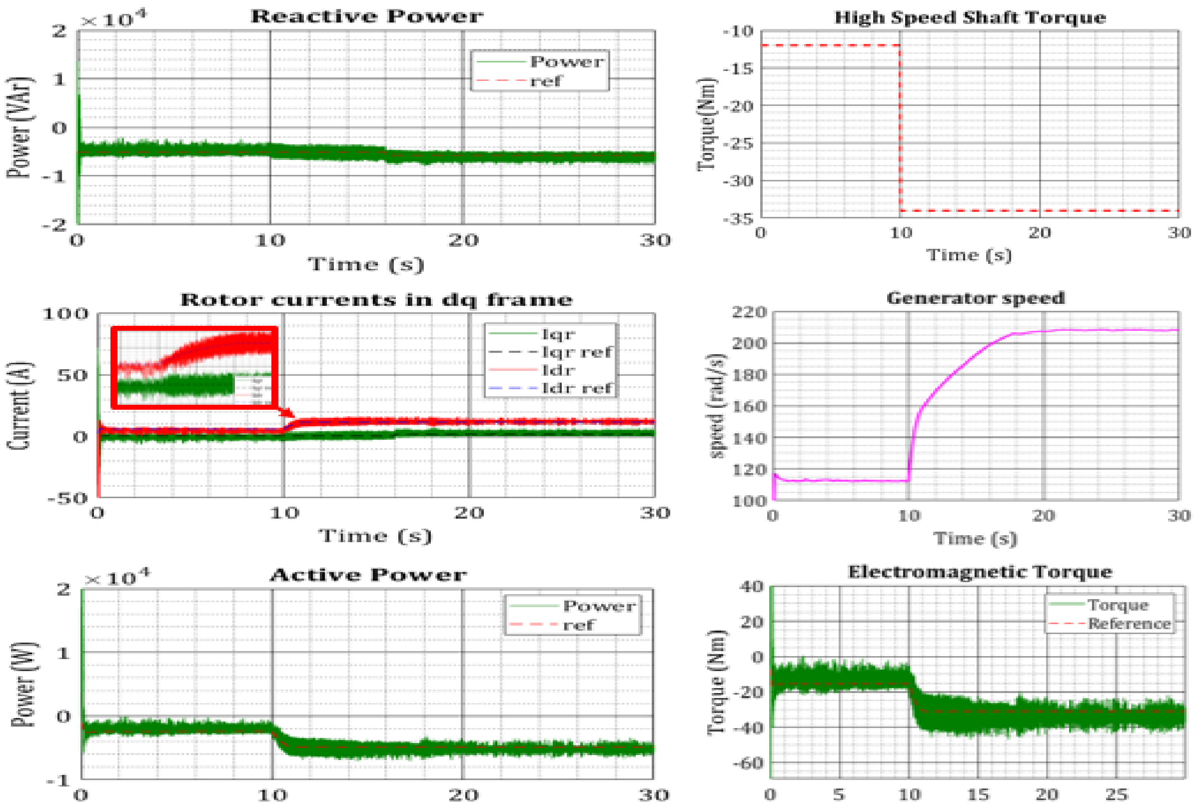

Fig. 6. Tracking performance of the self-scheduled controller.

The controller is tested for a torque variation of -12 to -34 Nm. This gives a generator speed of between 110 rad/s to 210 rad/s which represents about ±30% of the synchronous speed. The controller shows good response for the torque, power and the reference rotor currents in the *dq* frame. The controller is also stable throughout the range apart from guaranteeing good performance.

4.2 Tracking Performance of the Self-Scheduled Controller with the VAWT at Start-up

Since VAWTs are known to have poor self-starting performance, simulations were also included to study the self-starting characteristics of the VAWT and how fast the controller adapts. Figure 7 shows the behavior of the system during start-up and the adaptation of the self-scheduled controller to the start-up conditions.

4.3 Control at Rated Power by Torque Control

Fig. 8 shows the application of the torque control for power limitation at above rated wind speeds. Normally, this is partially achieved by pitch control and the use of torque control is an effective complement to it. The wind speed rises up to 16 m/s causing the speed of the rotor to rise along. The maximum torque for the generator is rated at 31 Nm. When this value is reached, an increase in the speed of the wind should cause no further increase in active power production.

The variables track the reference up to 12 s after which the controller can no longer force the torque to maintain at the rated values. This is a proof that torque control is not sufficient for power limitation above rated wind speeds.

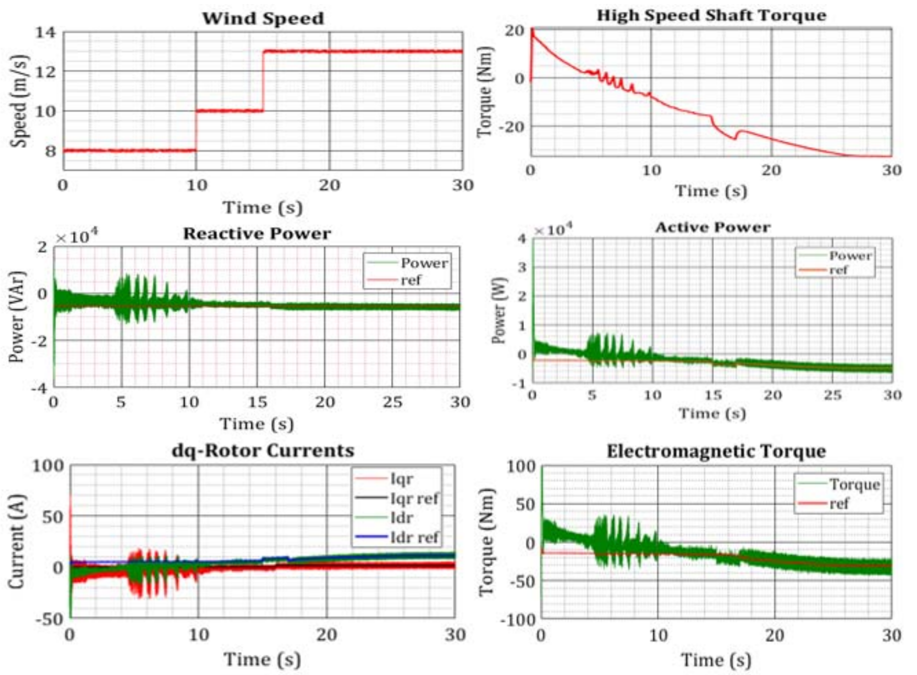

Fig. 7. Performance of the DFIG connected to the VAWT with start-up characteristics.

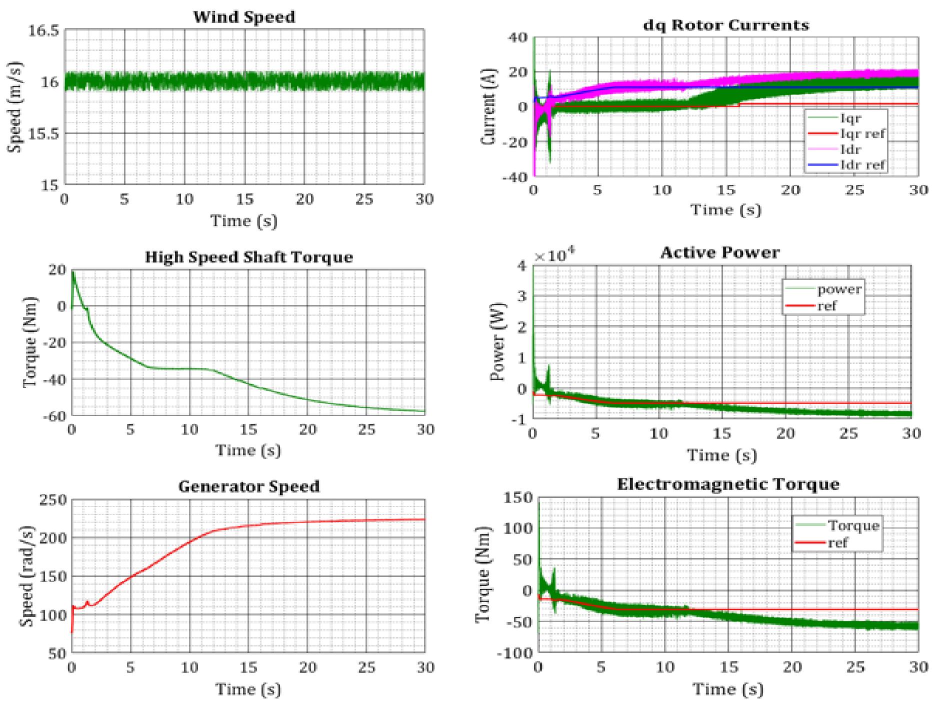

Fig. 8. Torque control of the VAWT above rated wind speeds.

4.4 Grid Frequency Support

Figure 7 also demonstrates the performance of the self-scheduled controller and behavior of the system for frequency support of the grid. At 15 s, a frequency drop of about 15 Hz is programmed to occur as seen in Fig.9. This causes the generator to demand more power to compensate for active power in the grid. The VAWT is slowed down as observed from the generator speed and the energy stored in the turbine inertia is momentarily used as back-up. The torque of the high-speed shaft shoots up and this provides extra active power as can be seen in Fig. 7. The controller shows quick response hence demonstrating good performance. The wind is maintained at rated speeds of 12 m/s corresponding to near synchronous speed for the DFIG.

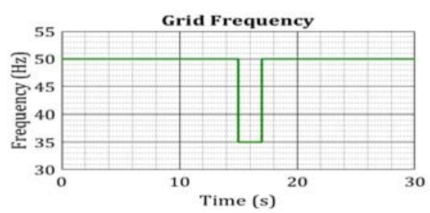

Fig. 9. Grid frequency fluctuation.

4.5 Tracking Comparison with PI Control

For similar conditions, of torque variation for the entire range of operation, as the self-scheduled controller in Fig. 7, the PI controller exhibits uncertain behavior as can be seen between 10 seconds and 12 seconds.

State changes in generator speeds also trigger big overshoots as observed at 18s in Fig. 10 for the *d-q* currents, power and electromagnetic torque.

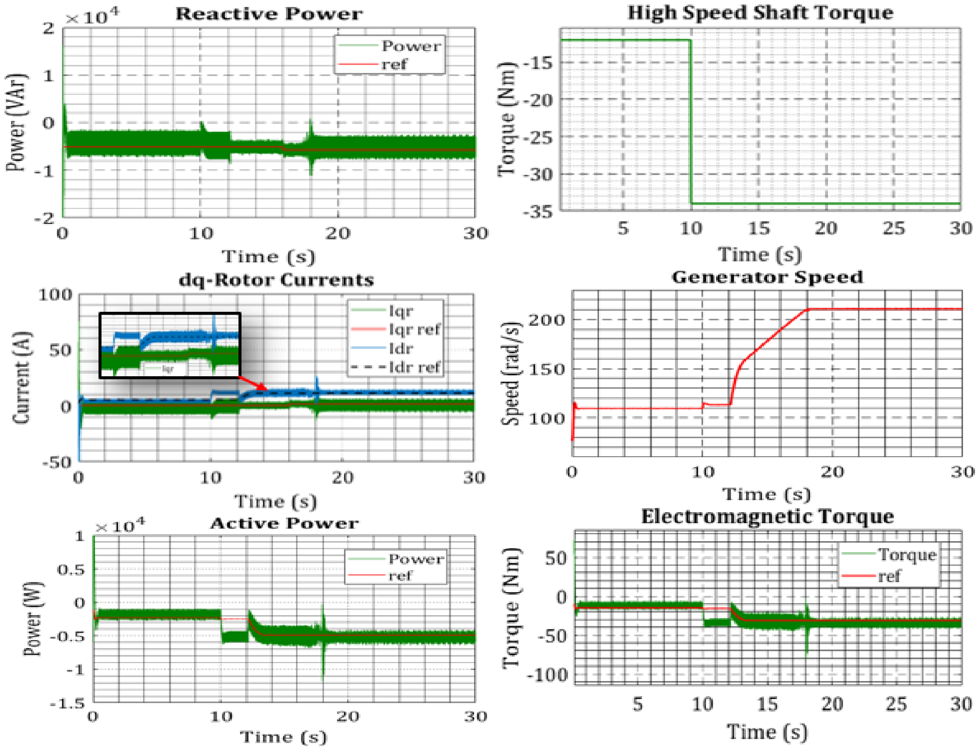

Fig. 10. Tracking performance of PI controller.

4.6 Tracking Performance of the PI Controller with the VAWT at Start-up

The PI controller shows poor tracking characteristics at start-up of the VAWT as shown in Fig. 11. Tracking performance is effected at about 24 seconds whereas the self-scheduled controller in Fig. 7 manages to effect tracking at about 12 s.

The PI controller however, does not introduce oscillations and overshoots as the high-speed shaft torque crosses from positive to negative as in Fig. 7.

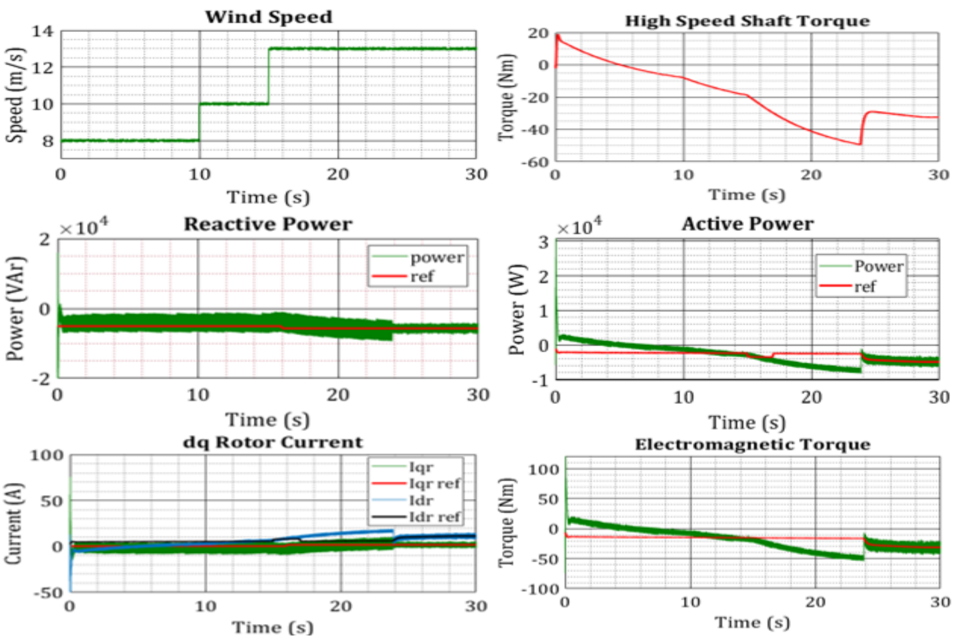

Fig. 11. Response of the PI controller to start-up conditions of the VAWT.

The PI controller however, does not introduce oscillations and overshoots as the high-speed shaft torque crosses from positive to negative as in Fig. 7.

5. CONCLUSION

The work has proposed a novel self-scheduled LPV control for a small scale vertical axis wind turbine (VAWT) based power plant. The system is tested against different demanding and realistic environmental conditions. This is characteristic of urban and sub-urban areas. The self-scheduled proposed controller guarantees a better performance compared to the classical PI control throughout the operation range. Despite the sudden torque variations, it is revealed that the control strategy involves insignificant overshoots. The set-up has also been used to demonstrate the application for frequency support and power limitation above rated conditions. Although the proposed set-up is successful for frequency support, it is not sufficient to apply torque control alone for power limitation above rated wind speeds. As a result, a pitch control is highly recommended as a supplement strategy for power control above rated wind speeds. The comparison with conventional PI controller indicates that the self-scheduled LPV control results into a superior decoupled performance with smaller overshoots and a quicker settling time. The study findings are critical to designers of wind turbines coupled with DFIGs for wind energy generation.

REFERENCES

Abdalrahman, G., Melek, W. & Lien, F.-S., 2017. Pitch angle control for a small-scale Darrieus vertical axis wind turbine with straight blades (H-Type VAWT). *Renewable energy,* 114**,** 1353-1362.

Apkarian, P. & Adams, R. J., 2000. Advanced gain-scheduling techniques for uncertain systems. *Advances in linear matrix inequality methods in control.* SIAM.

Apkarian, P., Gahinet, P. & Becker, G., 1995. Self-scheduled H∞ control of linear parameter-varying systems: a design example. *Automatica,* 31**,** 1251-1261.

Balduzzi, F., Bianchini, A., Maleci, R., Ferrara, G. & Ferrari, L., 2016. Critical issues in the CFD simulation of Darrieus wind turbines. *Renewable Energy,* 85**,** 419-435.

Boukhezzar, B. & Siguerdidjane, H. J. C. E. P., 2010. Comparison between linear and nonlinear control strategies for variable speed wind turbines. 18**,** 1357-1368.

Breslan, D., Apsley, J., Smith, A., Kirkham, S. & Towell, K., 2016. Control of a vertical axis wind turbine in gusty conditions.

Cárdenas, R., Peña, R., Alepuz, S. & Asher, G., 2013. Overview of control systems for the operation of DFIGs in wind energy applications. *IEEE Transactions on Industrial Electronics,* 60**,** 2776-2798.

Cheng, Z., Madsen, H. A., Gao, Z. & Moan, T., 2017. Effect of the number of blades on the dynamics of floating straight-bladed vertical axis wind turbines. *Renewable energy,* 101**,** 1285-1298.

Danao, L. A., Edwards, J., Eboibi, O. & Howell, R., = 2014. A numerical investigation into the influence of unsteady wind on the performance and aerodynamics of a vertical axis wind turbine. *Applied Energy,* 116**,** 111-124.

Gu, D.-W., Petkov, P. & Konstantinov, M. M., 2005. *Robust control design with MATLAB®*, Springer Science & Business Media.

Houpis, C. H. & Garcia-Sanz, M., 2012. *Wind energy systems: control engineering design*, CRC press.

Inthamoussou, F. A., Bianchi, F. D., DE Battista, H. & Mantz, R. J., 2014. LPV wind turbine control with anti-windup features covering the complete wind speed range. *IEEE Transactions on Energy Conversion,* 29**,** 259-266.

Inthamoussou, F. A., De Battista, H. & Mantz, R. J., 2016. LPV-based active power control of wind turbines covering the complete wind speed range. *Renewable energy,* 99**,** 996-1007.

Li, S., Challoo, R. & Nemmers, M. J. Comparative study of DFIG power control using stator-voltage and stator-flux oriented frames. 2009 IEEE Power & Energy Society General Meeting, 2009. IEEE, 1-8.

Merabet, A., Eshaft, H. & Tanvir, A. A., 2018. Power-current controller based sliding mode control for DFIG-wind energy conversion system. *IET Renewable Power Generation,* 12**,** 1155-1163.

Nguyen, L. & Metzger, M., 2017. Optimization of a vertical axis wind turbine for application in an urban/suburban area. *Journal of Renewable and sustainable Energy,* 9**,** 043302.

Onol, A. O. & Yesilyurt, S., 2017. Effects of wind gusts on a vertical axis wind turbine with high solidity. *Journal of Wind Engineering Industrial Aerodynamics* 162**,** 1-11.

Østergaard, K. Z., Stoustrup, J. & BRATH, P., 2009. Linear parameter varying control of wind turbines covering both partial load and full load conditions. *International Journal of Robust and Nonlinear Control: IFAC-Affiliated Journal,* 19**,** 92-116.

Polinder, H., Ferreira, J. A., Jensen, B. B., Abrahamsen, A. B., Atallah, K. & Mcmahon, R. A., 2013. Trends in wind turbine generator systems. *IEEE Journal of emerging selected topics in power electronics,* 1**,** 174-185.

Ramtharan, G., Jenkins, N. & Ekanayake, J., 2007. Frequency support from doubly fed induction generator wind turbines. *IET Renewable Power Generation,* 1**,** 3-9.

Rezaeiha, A., Kalkman, I. & Blocken, B., 2017. Effect of pitch angle on power performance and aerodynamics of a vertical axis wind turbine. *Applied energy,* 197**,** 132-150.

Smajo, J. & Vukadinovic, D., 2008. Electromagnetic torque analysis of a DFIG for wind turbines. *WSEAS Transactions on Systems,* 7**,** 479-488.

Tien, H. N., Scherer, C. W., Scherpen, J. M. & Müller, V., 2016. Linear parameter varying control of doubly fed induction machines. *IEEE Transactions on industrial electronics* 63**,** 216-224.

Vas P., 1998. *Sensorless vector and direct torque control*, Oxford Univ. Press.

Wang, C. & Weiss, G., 2014. Linear parameter varying control of a doubly fed induction generator based wind turbine with primary grid frequency support. *International Journal of Robust Nonlinear Control* 24**,** 1927-1946.

Wang, Y., Wu, Q., Gong, W. & Gryning, M. P. S., 2016. H-infinity Robust Current Control for DFIG-Based Wind

Turbine Subject to Grid Voltage Distortions. *IEEE Transactions on Sustainable Energy,* 8**,** 816-825.

Wekesa, D. W., Wang, C., Wei, Y. & Danao, L. A. M., 2017. Analytical and numerical investigation of unsteady wind for enhanced energy capture in a fluctuating free-stream. *Energy,* 121**,** 854-864.

Wekesa, D. W., Wang, C., Wei, Y. & Zhu, W., 2016. Experimental and numerical study of turbulence effect on aerodynamic performance of a small-scale vertical axis wind turbine. *Journal of Wind Engineering and Industrial Aerodynamics,* 157**,** 1-14.

Willems, J., 1971. Least squares stationary optimal control and the algebraic Riccati equation. *IEEE Transactions on Automatic Control,* 16**,** 621-634.

Wong, K. H., Chong, W. T., Sukiman, N. L., POH, S. C., Shiah, Y.-C. & Wang, C.-T., 2017. Performance enhancements on vertical axis wind turbines using flow augmentation systems: A review. *Renewable and Sustainable Energy Reviews* 73**,** 904-921.